Available online at [www.sciencedirect.com](http://www.sciencedirect.com)

ScienceDirect

[www.elsevier.com/locate/jmbbm](http://www.elsevier.com/locate/jmbbm)

## Technical Note

# A methodology for the investigation of toughness and crack propagation in mouse bone



Alessandra Carriero<sup>a,b,c,\*</sup>, Elizabeth A. Zimmermann<sup>b,c</sup>,  
Sandra J. Shefelbine<sup>a,1</sup>, Robert O. Ritchie<sup>b,c,1</sup>

<sup>a</sup>Department of Bioengineering, Imperial College London, London, UK

<sup>b</sup>Materials Sciences Division, Lawrence Berkeley National Laboratory, Berkeley, USA

<sup>c</sup>Department of Materials Science and Engineering, University of California Berkeley, USA

## ARTICLE INFO

## Article history:

Received 6 March 2014

Received in revised form

22 June 2014

Accepted 27 June 2014

Available online 9 July 2014

## Keywords:

Bone fracture

Mouse bone

Fracture mechanics

Crack path

Crack initiation

Brittle bone

Crack growth

## ABSTRACT

Bone fracture is a health concern for those with aged bone and brittle bone diseases. Mouse bone is widely used as a model of human bone, especially to investigate preclinical treatment strategies. However, little is known about the mechanisms of mouse bone fracture and its similarities and differences from fracture in human bone. In this work we present a methodology to investigate the fracture toughness during crack initiation and crack propagation for mouse bone.

Mouse femora were dissected, polished on their periosteal surface, notched on the posterior surface at their mid-diaphysis, and tested in three-point bending under displacement control at a rate of 0.1 mm/min using an *in situ* loading stage within an environmental scanning electron microscope.

We obtained high-resolution real-time imaging of the crack initiation and propagation in mouse bone. From the images we can measure the crack extension at each step of the crack growth and calculate the toughness of the bone (in terms of stress intensity factor ( $K$ ) and work to fracture ( $W_f$ )) as a function of stable crack length ( $\Delta a$ ), thus generating a resistance curve for the mouse bone.

The technique presented here provides insight into the evolution of microdamage and the toughening mechanisms that resist crack propagation, which are essential for preclinical development of treatments to enhance bone quality and combat fracture risk.

© 2014 Elsevier Ltd. All rights reserved.

\*Corresponding author at: Department of Bioengineering, Royal School of Mines, Imperial College London, South Kensington Campus, SW7 2AZ London, UK. Tel.: +44 791 454 2255.

E-mail address: [a.carriero@imperial.ac.uk](mailto:a.carriero@imperial.ac.uk) (A. Carriero).

<sup>1</sup>These authors contributed equally to this work.

## 1. Introduction

The mechanical properties of bone are determined by its composition and structure over many length-scales, and influenced by the loads it supports through adaptation and remodelling. The structural integrity of the bone is therefore of great clinical importance for preserving its function and adaptability. Aging and diseases, such as osteoporosis, osteogenesis imperfecta and vitamin-D deficiency, change the bone-matrix structure, which can degrade its material properties, thereby promoting its vulnerability to fracture (Busse et al., 2013; Carriero et al., 2014a, 2014b). In the case of the elderly and in severe conditions of brittle bone diseases, these changes are often critical as subsequent fractures can be the cause of mortality.

Traditionally, bone quantity has been considered to be a predictor of bone fracture risk; specifically an increased rate of fracture in aged and diseased bones has been primarily associated with low bone mass or low bone mineral density (BMD, defined by the amount of bone mineral per unit cross-sectional area). Although low bone mass can explain some of the increases in fracture rates, there is increasing evidence that bone mass alone is not the sole factor responsible for aging- or disease-induced fracture risks (Hui et al., 1988; Aspray et al., 1996; Heaney, 2003). Furthermore, BMD alone cannot explain medical benefits of therapies, such as anti-resorptive agents, in treating porous bone (Riggs et al., 1996; Heaney, 2003). For these reasons, there has been a renewed interest in factors controlling bone quality, i.e., structure, porosity, composition, strength and specifically bone toughness.

Encouraged by the idea that an accurate evaluation of bone quality could potentially be a predictor of risk of bone fracture, recent studies on the fracture properties of bone (Ziopoulos et al., 1996; Vashishth et al., 1997; Yeni et al., 1997; Ziopoulos 1999; Nalla et al., 2003, 2005, Kruzic et al., 2005 Peterlik et al., 2006; Koester et al., 2008) have focused on understanding the origin of bone toughness and its resistance to crack propagation in relation to bone's multi-scale structure. Bone is a complex hierarchical composite of collagen and hydroxyapatite, which forms different structures at several dimensional scales. At the nanoscale, cortical bone is composed of mineralized type I collagen fibrils, bundled together in fibers and filled with carbonate apatite nanocrystals. These fibers are further organized into a lamellar structure at the microscale. Oriented along the long axis of human bone at the scale of hundreds of microns, there are the osteons which are composed of circumferential lamellar rings that surround large vascular channels; their boundaries are delineated by hypermineralized layers known as cement lines.

This complex hierarchical structure dictates the mechanical properties of bone and specifically how cracks propagate through it during fracture. It has been shown that at each hierarchical level, toughening mechanisms resist the initiation and growth of cracks (Launey et al., 2010). At the smallest (nanoscale) length-scales, mechanisms such as collagen uncoiling and fibrillar sliding contribute to bone's ability to absorb energy during deformation and fracture (i.e., intrinsic

toughness<sup>2</sup>), while at larger length scales, mechanisms such as crack deflection and uncracked-ligament bridging interact with the growing crack to increase the bone's resistance to crack growth (i.e., extrinsic toughness) (Launey et al., 2010). Previous studies have focused on the origin of human bone's fracture resistance in relation to the structural length scales and found that the toughness of bone at macroscopic levels displays a rising resistance-curve (R-curve) behavior<sup>3</sup> where the fracture resistance increases during the process of crack extension (Vashishth et al., 1997, 2003; Nalla et al., 2004a, 2005; Koester et al., 2008). This increase in toughness with crack growth is indicative of the presence of extrinsic toughening mechanisms, which act predominantly in the crack wake. In bone, the primary extrinsic toughening mechanisms resulting in R-curve behavior are crack deflection and the formation of uncracked-ligament bridges (Koester et al., 2008; Launey et al., 2010).

Despite the current understanding of the origins and mechanisms of toughening in human bone, it is still not fully understood how specific disease states can affect these mechanisms and how certain therapies can improve bone toughness to reduce the fracture risk. In this latter context, animal models of human bone are routinely used to predict the outcome of therapies in humans. An understanding of how fracture mechanisms change for different bone diseases and with different therapies is critical to the design of effective treatments.

Mouse models mimicking biochemical and phenotypic features of human forms of different bone diseases offer a viable pathway to explore how bone fractures at all of its structural levels and to enhance preclinical testing of therapies that can help restore toughness in bone and reduce its fracture risk. Recently, Ritchie et al. (2008) provided a suite of procedures for defining the toughness of mouse bone using single-value characterizations of the fracture toughness, specifically by using the parameters  $K_c$  and  $J_c$ .<sup>4</sup> However, there is still a very limited

<sup>2</sup>Intrinsic toughening mechanisms operate ahead of the crack tip to generate resistance to microstructural damage. The most prominent mechanism is that of plastic deformation which provides a means of blunting the crack tip through the formation of "plastic" zones. Extrinsic toughening mechanisms, conversely, operate primarily in the wake of the crack tip to inhibit cracking by "shielding" the crack from the applied driving force (Launey et al., 2010). Whereas intrinsic toughening mechanisms are effective in inhibiting both the initiation and growth of cracks, extrinsic mechanisms, e.g., crack bridging, are only effective in inhibiting crack growth.

<sup>3</sup>The crack resistance- or R-curve provides an assessment of the fracture toughness in the presence of subcritical crack growth. It involves measurements of the crack-driving force, e.g., the stress intensity  $K$ , strain-energy release rate  $G$  or  $J$ -integral, as a function of crack extension ( $\Delta a$ ). The value of the driving force at  $\Delta a \rightarrow 0$  provides a measure of the crack-initiation toughness whereas the slope and/or the maximum value of the R-curve can be used to characterize the crack-growth toughness.

<sup>4</sup>Based on linear-elastic fracture mechanics (LEFM), the stress-intensity factor  $K$  characterizes the local distribution of stress and displacement in the vicinity of a sharp crack in a linear-elastic solid. It is determined by  $K = Y\sigma_{app}(\pi a)^{1/2}$  where  $\sigma_{app}$  is the applied stress,  $a$  is the crack length, and  $Y$  is a function (of order unity) of crack size and geometry. In the presence of more extensive inelasticity, an alternative crack-driving "force" can be expressed in terms of the so-called  $J$ -integral, which is defined as the change in potential energy per unit increase in crack area in a nonlinear

understanding of the mechanics of mouse bone fracture in relation to its hierarchical, multidimensional structure, especially with respect to the partitioning of crack initiation vs. crack growth (as achieved using an R-curve characterization) and how these findings relate to crack propagation in human bone. Mouse bone structure differs from humans in that it does not have osteons nor Haversian canals but only lamellae surrounding the central medullary cavity, which contribute to mouse bone anisotropic material properties (Saban et al., 1996). Studies have shown that in human bone the osteonal structure and cement lines around osteons are critical to crack propagation behavior, particularly in crack deflection (Zioupos and Currey 1994; Nalla et al., 2004b; Koester et al., 2008; Launey et al., 2010). Therefore, one vital question is: how is toughness achieved in mouse bone that lacks the osteonal structure?

In this study, we present a fracture mechanics methodology to investigate the toughness of mouse bone, by monitoring the extension of stable crack growth in mouse femora by simultaneously imaging the crack path during toughness measurements to discern the sources of toughness. Specifically, we have measured the crack-initiation toughness and crack-resistance curve (R-curve) in mouse bone, using *in situ* measurements in an environmental scanning electron microscope (ESEM) to identify the salient damage and toughening mechanisms. This methodology has been applied to mouse models of brittle osteogenesis imperfecta *oim* bone disease and to the respective wild type (WT) mouse model, allowing us to identify differences in the mechanisms of fracture toughness between normal bone and more brittle bone (Carriero et al., 2014b). In this manuscript we present the technique in detail. Calculating the toughness of bone during crack growth and understanding of how mouse bone resists such fracture can provide vital information about the mechanical properties of the bone for the investigation of diseased conditions and of treatments aimed at improving bone frailty to reduce fracture risk.

## 2. Methods

Using three test samples from a heterozygous mouse model of osteogenesis imperfecta disease, B6C3 Fe-a/col1a2<sup>oim/+</sup> (*oim*/+), and respective wild type (WT) from our previous study (Carriero et al., 2014b), we here present the technique that we used to characterize the onset of cracking and its subsequent propagation in brittle and healthy mouse bones. These two types of bones were specifically chosen to present this methodology as they have statistically different fracture toughness (Carriero et al., 2014b) due to dissimilar cortical bone hierarchical structures: the WT mice have very organized cortical bone with concentric lamellar rings around the marrow cavity, and few vascular canals, while the *oim*/+ mice have highly disorganized cortical bone with very little lamellar bone and many branched vascular channels (Saban et al., 1996; Carriero et al., 2014a). Here the results from these two groups of bones are utilized to show the advantages of the techniques and how to validate their results.

(footnote continued)

elastic solid. Critical values of these  $K$  and  $J$  parameters at the onset of fracture, namely  $K_c$  and  $J_c$ , can be used as measure of the material's fracture toughness.

Fresh frozen femora of three *oim*/+ and three WT mice, all eight weeks old and male, were dissected for testing. The periosteal surface of the femora was then polished starting with 400 grit silicon carbide paper to an increasingly higher finish until a final polish with 0.5  $\mu\text{m}$  diamond suspension to make the osteocyte lacunae and the canals visible within the environmental scanning electron microscope (Hitachi S-4300SE/N ESEM, Hitachi America, Pleasanton, CA). The samples were then machine micro-notched on the posterior surface of the mid-diaphysis with a razor blade irrigated with 0.05  $\mu\text{m}$  diamond suspension; notch root radii with this technique consistently were less than 10  $\mu\text{m}$ <sup>5</sup>. To preserve the material properties of the bone, the femora were immersed in ambient Hanks' Balanced Salt Solution (HBSS) for at least 12 h prior to testing. To define changes in the crack initiation and subsequent crack paths at the microstructural level in the two mouse models, crack propagation was observed in the ESEM while bones were tested in three-point bending with a span of 6 mm (span/femur radius ratio of  $\sim 4$ ) using a Gatan Microtest 2-kN three-point bending stage (Gatan, Abington, UK); measurement procedures were in general accordance with those described by Ritchie et al. (2008) (Fig. 1a). Before loading in the rig, the femur was examined under an optical microscope to ensure that the notch was centered between the loading pins, and had equal length on the lateral sides of the bone. This ensures that the crack grows simultaneously on both sides of the bone. The femoral bones were loaded moist under displacement control at a rate of 0.1 mm/min at 25 °C on the *in situ* loading stage in variable pressure mode within the ESEM. Images of the crack path were obtained simultaneously in back-scattered mode at 25 kV with a pressure of 35 Pa.

The ESEM images of the crack growth permitted the measurement of the toughness at each increment of stable crack extension. Consequently, fracture toughness crack-resistance curves (R-curves) for stable crack propagation in the mouse bone were determined in terms of the stress-intensity factor,  $K$ , characterizing the toughness as a function of crack extension,  $\Delta a$ .<sup>6</sup> Fracture toughness values were

<sup>5</sup>Generating an atomically-sharp notch is important as in the stress intensity developed at a notch can be severely reduced if the stress concentrator is not sharp (the value of the stress intensity  $K$  is decreased by an amount inversely proportional to the square-root of the radius of the notch) (Ritchie et al., 2008). It is however, not easy to generate an atomically-sharp notch in small biological specimen because the technique of fatiguing in a starter crack requires precise control for specimen and constraint at the crack tip to prevent changes to the bulk material. This is even more complicated in mouse bone with a tubular and not perfectly cylindrical geometry. Previous studies have shown that notches with root radii of  $\sim 10 \mu\text{m}$  are generally obtained with a notching machine and that this is very slightly going to influence the  $K$  value. In this study, we have used a notching machine for notching our bones and made sure that the notch radius was always less than 10  $\mu\text{m}$ .

<sup>6</sup>While a nonlinear  $J$ -integral analysis may provide a more appropriate characterization of toughness at larger crack extensions, a LEFM analysis was used here as currently a  $J$ -integral solution does not exist for the geometry of thick-walled circular cylinder, pertaining to that of mouse bone (Ritchie et al., 2008).

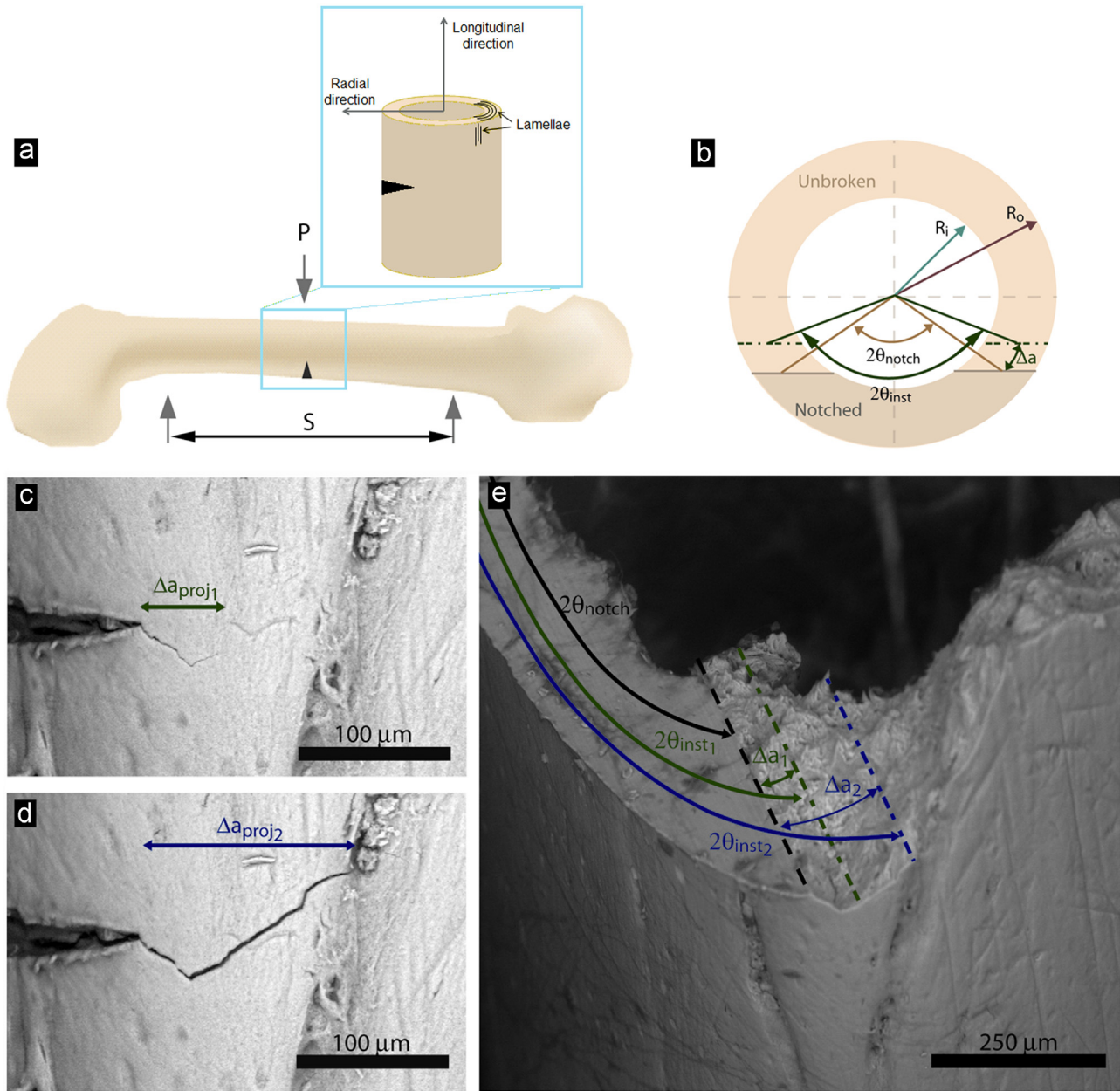


**Fig. 1 – (a)** Fracture toughness testing was performed on whole HBSS-saturated mouse femurs with a through-thickness sharp notch on the posterior side loaded in three-point bending in the ESEM. The zoomed schematic on the side shows the presence of lamellae in WT mouse bone, which contribute to its anisotropy. **(b)** The fracture toughness  $K_c$  was measured as the stress intensity at the onset of cracking or its continuation, using the linear-elastic solution for a cylindrical pipe with a through-thickness sharp notch. Measurements of the inner radius,  $R_i$ , and outer radius,  $R_o$ , of the bone as well as the half-crack angles of the notch and instantaneous crack growth,  $\theta_{notch}$  and  $\theta_{inst}$ , respectively, allowed the calculation of the toughness.  $\theta_{notch}$  represents the half-crack angle prior to loading and crack growth. **(c and d)** As the bone was loaded in the ESEM, the progress of crack growth was imaged; the crack extension was measured along a straight path from the notch root,  $\Delta a_{proj}$ . After testing,  $\theta_{inst}$  was determined by imaging the fracture surface **(e)** and relating this to the lateral surface of the bone in order to estimate the instantaneous half-crack angle for each increment in crack growth.

computed using the linear elastic fracture mechanics (LEFM) stress-intensity solution for a through-thickness crack in a circular thick-walled cylinder:

$$K = F_b \frac{PSR_o}{\pi(R_o^4 - R_i^4)} \sqrt{\pi R_m \theta_{inst}}$$

where  $F_b$  is a geometric constant for thick-walled cylinders,  $P$  is the instantaneous load,  $S$  is the span width,  $R_m$ ,  $R_i$  and  $R_o$  are the mean, inner and outer radius of the bone, respectively, and  $\theta_{inst}$  is the instantaneous instability half-crack angle, given that  $\theta_{inst}$  is smaller than  $220^\circ$  (Zahoor 1989, Ritchie et al., 2008) (Fig. 1a and b). The geometric constant

$F_b$  for thick-walled cylinders is defined as:

$$F_b = \left(1 + \frac{t}{2R_m}\right) \left[ A_b + B_b \left(\frac{\theta}{\pi}\right) + B_b \left(\frac{\theta}{\pi}\right) + C_b \left(\frac{\theta}{\pi}\right)^2 + D_b \left(\frac{\theta}{\pi}\right)^3 + E_b \left(\frac{\theta}{\pi}\right)^4 \right]$$

Where

$$A_b = 0.65133 - 0.5774\varepsilon - 0.3427\varepsilon^2 - 0.0681\varepsilon^3$$

$$B_b = 1.879 + 4.795\varepsilon + 2.343\varepsilon^2 - 0.6197\varepsilon^3$$

$$C_b = -9.779 - 38.14\varepsilon - 6.611\varepsilon^2 + 3.972\varepsilon^3$$

$$D_b = 34.56 + 129.9\varepsilon + 50.55\varepsilon^2 + 3.374\varepsilon^3$$

$$E_b = -30.82 - 147.6\varepsilon - 78.38\varepsilon^2 - 15.54\varepsilon^3$$

$$\varepsilon = \log\left(\frac{t}{R_m}\right)$$

with  $t$  being the mean thickness of the cylinder.

During ESEM testing, the instantaneous load,  $P$ , was recorded with ESEM images of the lateral surface of the bone used to measure the chord of the instantaneous crack extension,  $\Delta a_{proj}$ , considered not along its deflected path, but as if projected along a transverse/horizontal line starting from the notch root (Fig. 1c and d).

To determine the geometrical characteristics of the bone and the instantaneous half-crack angle,  $\theta_{inst}$ , the fracture surfaces of the fully broken samples were imaged in back-scattered mode in the ESEM after testing; this permitted the incremental projected crack length,  $\Delta a_{proj}$ , to be related to the instability angle,  $\theta_{inst}$ , through the circumferential crack extension,  $\Delta a$ , (Fig. 1e). The value of the instantaneous crack extension,  $\Delta a$ , was geometrically calculated along the circumference of the bone with mean radius as for the formula:

$$\Delta a = \frac{2\pi(R_o - R_i)(\theta_{inst} - \theta_{notch})}{360}$$

where  $\theta_{notch}$  is the half-notch angle.

For the LEFM measurements, the deformation is assumed to be linear elastic, i.e., the crack-tip plastic zone in the plane of the crack and through the thickness must be small enough to be ignored (i.e., a state of, respectively, small-scale yielding and plane strain prevails). The plastic-zone size can be estimated by:

$$r_y \sim \left(\frac{1}{2\pi}\right) \left(\frac{K}{\sigma_y}\right)^2$$

where  $K$  and  $\sigma_y$  are, respectively, the stress intensity and yield stress (with  $\sigma_y \sim 100$  MPa). If the plastic-zone size is roughly an order of magnitude smaller than the in-plane dimensions of the crack size ( $\Delta a$ ), remaining uncracked ligament ( $\Delta b = 2R_o - \Delta a$ ) and specimen dimensions (width, length, mean radius, twice its mean thickness—because crack propagates in the two parts equally), then a state of small-scale yielding can be deemed to exist. Finally, for the validity of the R-curves for the K-values, measurements must be taken only up to a maximum crack extension  $\Delta a_{max} < 0.25 b_0$ , where  $b_0$  is the initial uncracked ligament as per above (ASTM E1820-09).

As measurements of fracture toughness  $K$  rely on isotropic LEFM-based mechanics solutions, which assume that contribution from plastic (inelastic) deformation and anisotropy are minimal (Feerick et al., 2013), we attempted to account for the additional contribution of inelastic deformation and anisotropy by also measuring R-curves in terms of the energy associated with cracking. We achieved this by measuring a second set of R-curves for the same mouse bones computed in terms of work

of fracture  $W_f$  as function of crack extension,  $\Delta a$ . The work to fracture essentially quantifies the energy expended to create two new surfaces and can be calculated as follows:

$$W_f = \frac{E_f}{2A_{res}}$$

where  $E_f$  is the energy of fracture (i.e., the instantaneous area under the load-displacement curve) and  $A_{res}$  is the area of the bone surface resisting the crack propagation, i.e., the total area of the bone minus the notch area.<sup>7</sup> The values  $K$  and  $W_f$  as a function of  $\Delta a$  provided a characterization of the bone toughness during stable crack growth, and as such could be used to estimate the elastic and inelastic contributions to toughness.

### 3. Results

High-resolution real-time ESEM images revealed large crack deflections in WT bone (Fig. 2a–h) and nearly straight crack propagation in *oim/+* bone (Fig. 2i–l). This resulted in a substantial increase of the fracture toughness as function of the crack extension in the WT bone but not in the *oim/+* bone (Fig. 3). The degree of toughening with crack extension (slope of the R-curve) in WT mouse bone is large: the toughness increases by 50% after 200  $\mu\text{m}$  of crack growth (Fig. 3), concomitant with mechanisms of crack deflection on the lateral surface of the bone (Fig. 2a–h). Crack deflections in WT bone were on the order of  $\sim 90^\circ$  for tens to hundreds of micrometers, in the longitudinal direction, before the cracks reinitiated at a much higher applied load and continued their tortuous paths along the nominal transverse direction (Fig. 2a–h and Fig. 3 Wild Type). This process was repeated several times during the extension of the stable crack growth and represents a significant mechanism of (extrinsic) toughness (a deflection through  $\sim 90^\circ$  can effectively double the toughness of the bone). In contrast, corresponding fracture in brittle *oim/+* bone required a lower driving force to initially extend the crack, which catastrophically broke after 200  $\mu\text{m}$  of stable crack growth (Fig. 3 *oim/+*), consistent with quasi-linear and almost undeflected crack profiles (Fig. 2i–l). It is apparent that for both WT and more brittle *oim/+* bone, cracks initiated at the root of the micro-notch and were not influenced by the vascular canals (Fig. 4).

The validity of the LEFM approach was maintained for the entire R-curves for K-values of the *oim/+* bone, where the plastic-zone size is roughly an order of magnitude smaller than the dimensions of the bone (i.e., length, diameter and cortical thickness), crack length and remaining uncracked ligament. In the WT bones, the cortical bone is very thin such that a state of small-scale yielding cannot be ensured throughout all of the experiment. Finally, according to the ASTM E1820-09, the validity of the R-curves for both K-values is restricted to  $\Delta a < 430 \mu\text{m}$  for *oim/+* bones and to  $\Delta a < 450 \mu\text{m}$  for WT bones. Valid measurements are reported with a continuous line in the R-curves represented in Fig. 3a.

<sup>7</sup>Interestingly, for a solid sample in pure bending, the work of fracture so calculated is directly proportional to the value of the J-integral, differing only by a small numerical factor of 4.

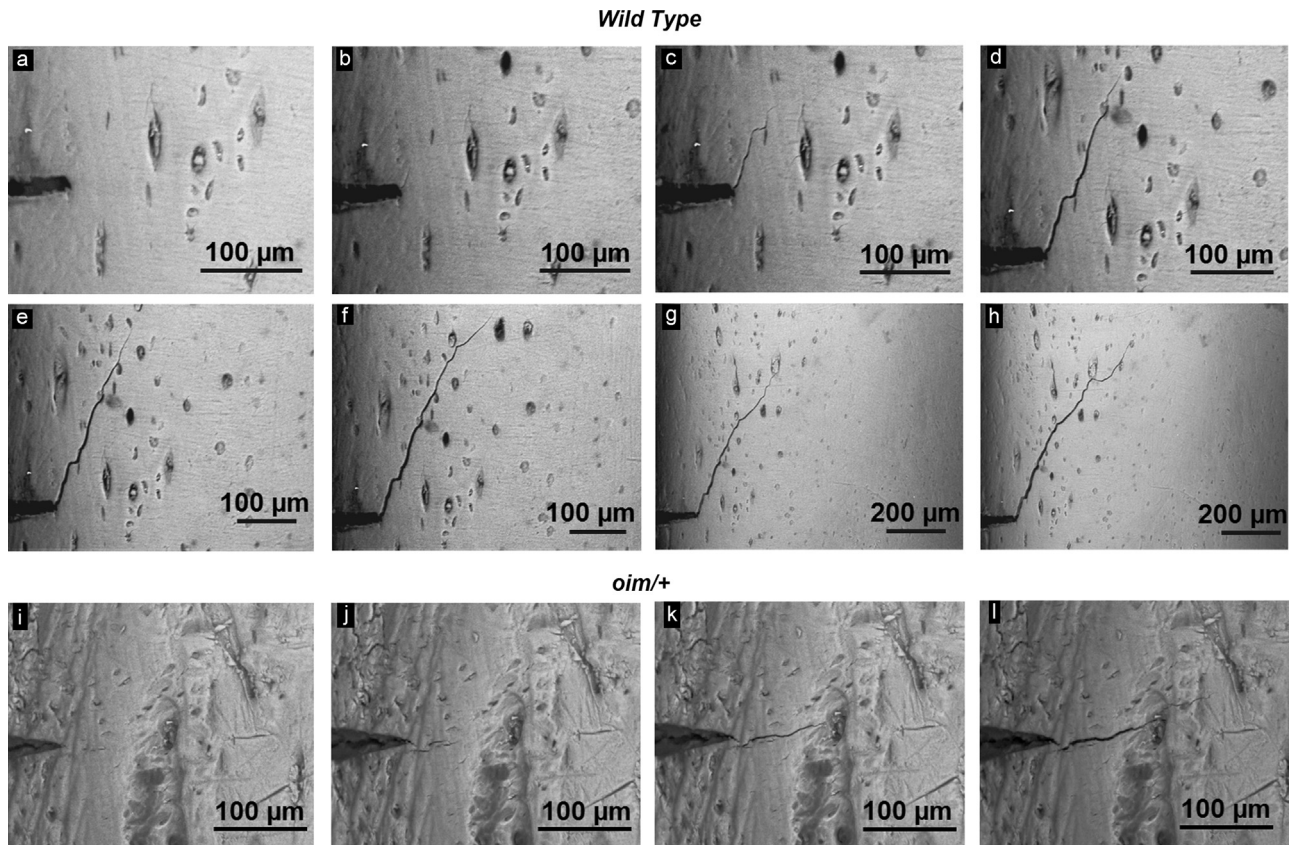


**Fig. 2 – ESEM images of the crack path taken over time of a single representative WT and *oim/+* mouse bone highlighting the differing mechanisms of toughening in the healthy and diseased bone. (a–h) Crack paths in WT bone underwent multiple crack deflections (c–f), which in conjunction with the through-thickness crack twists, resulted in a significant increase in bone toughness with crack extension - rising R-curve behavior (Fig. 3 WT). (i–l) Crack paths for *oim/+* bone, conversely, did not deflect and twist as in the WT bone, resulting in a 35% lower fracture toughness (Fig. 3 *oim/+*).**

#### 4. Discussion

In this study, a method for the characterization of the fracture resistance of mouse bone as a function of stable crack extension, i.e., based on the measurement of the R-curve, has been presented. The approach allows the comparison of bone toughness from different mice models of diseases, therapeutic treatments or transgenic mutations, and to discern the microstructural mechanisms causing the changes in bone toughness with the condition. This technique offers therefore advantages to the previously established models that define a single-value toughness in mouse bone (Ritchie et al., 2008), because it permits characterization of the effect of the crack path in the form of the crack-resistance curve to define the crack initiation and growth toughness, thereby providing details of the behavior of the crack in relation with the structure of bone at the microscopic level. In this manuscript, we used this methodology to measure the crack-resistance curve for two different types of bone (ductile and brittle). WT mouse bone exhibited a steeply rising R-curve with the crack path displaying crack deflections and twists, which are potent (extrinsic) toughening mechanisms typical of fracture behavior in human cortical bone (in the transverse orientation) (Koester et al., 2008). Conversely,

brittle *oim/+* bone did not exhibit such mechanisms to resist crack growth, with cracks propagating more rapidly in the transverse direction with little to no evidence of deflection, the resulting lack of extrinsic toughening in the diseased bone being consistent with an almost flat R-curve. However, in both the WT and *oim/+* mouse bone, crack growth was not markedly influenced by the presence of canals. Our use of *in situ* toughness testing in the ESEM investigation offers the opportunity to inspect the evolution of cracking on the external surface of a full mouse bone. It represents, of course, a two-dimensional imaging technique; three-dimensional imaging of damage and fracture in mouse bone can be achieved, with slightly lower spatial resolution, using synchrotron x-ray computed tomography (SR CT). In previous studies, mouse bone has been loaded in compression in a SR CT to characterize the initiation and propagation of microcracks and define the nature of microdamage in bone (Voide et al., 2009, Christen et al., 2012). This method provides a 3-D morphological characterization of the microcrack damage in relation to the cortical bone microstructure (Voide et al., 2009) and strain distribution (Christen et al., 2012), but does not provide measurements of the bone toughness and its evolution in relation to the crack path and extension. Furthermore, such *in situ* testing of bone is not always advisable as the radiation levels required for tomographic

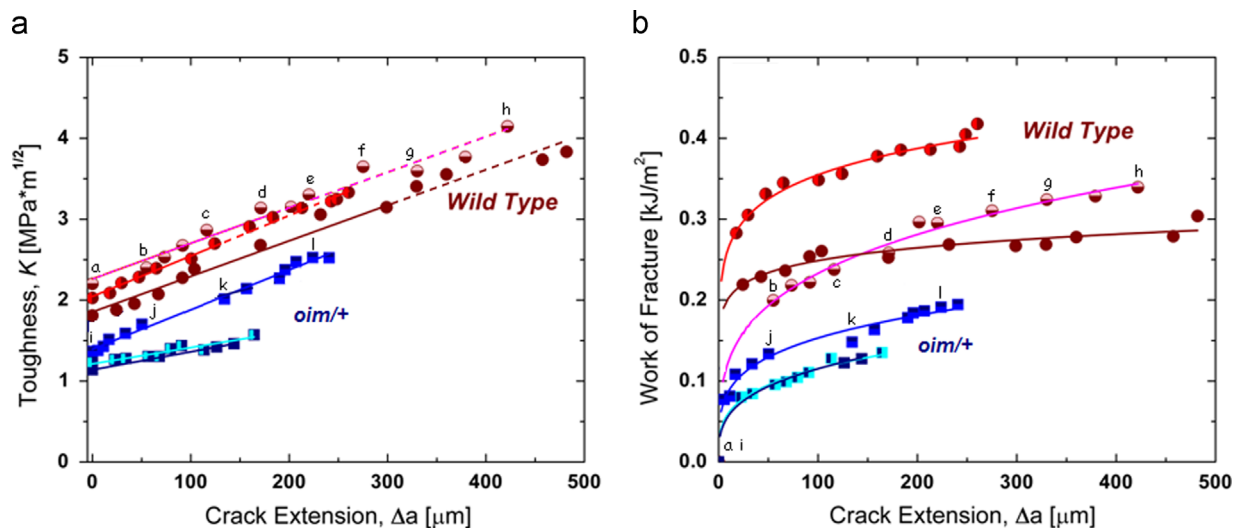


Fig. 3 – Crack-resistance curves (R-curves) for stable crack length showing the fracture resistance with crack extension in terms of the stress intensity  $K$  and the work of fracture  $W_f$ , for WT (red) and *oim/+* (blue) mouse bone (adapted from [Carriero et al. \(2014b\)](#)). WT mouse bone principally derives its toughness during crack growth and involved marked deflection of the crack path (Fig. 2), while brittle *oim/+* bone displayed a much more linear (undeflected) crack path. The small insert letters/numbers along the R-curves correlate the value of bone toughness to the instantaneous crack extension path as shown in Fig. 2, allowing direct relationship between crack growth and bone toughness. The validity of the stress intensity data, represented by a continuous curve, is defined by the small scale yielding and by the measurement capability of each sample in accordance of the ASTM standards (ASTM E1820-09) for the  $K$ -values. (For interpretation of the references to color in this figure legend, the reader is referred to the web version of this article.)

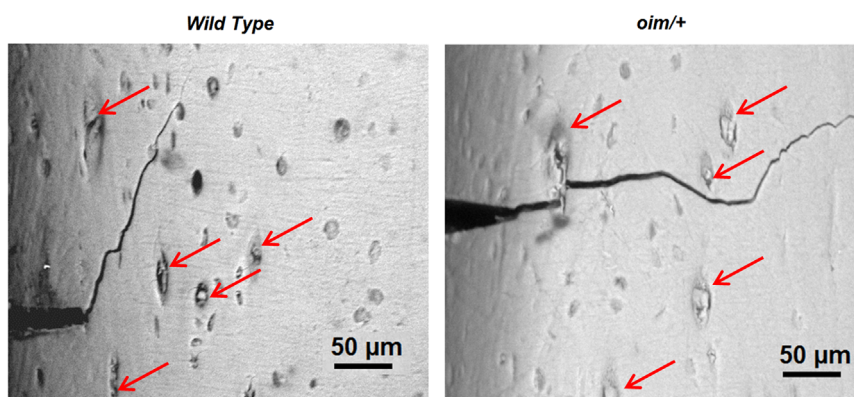


Fig. 4 – High resolution ESEM images of WT and *oim/+* bone showing that crack is not influenced by the presence of the canals, indicated by the red arrows. (For interpretation of the references to color in this figure legend, the reader is referred to the web version of this article.)

imaging can adversely affect the structure and properties of the bone ([Barth et al., 2010](#)).

Classical indentation methods have also been used to determine bone toughness as function of the crack length generated into the bone by a sharp diamond indenter, together with the elastic modulus and the hardness of the bone ([Kruzic et al., 2009](#)). Although less invasive than standard toughness measurement methods, the indentation methods are not always accurate in quantifying fracture toughness or crack growth toughness or in ranking the relative toughness of different biomaterials ([Kruzic et al., 2009](#)). The novel micro-indentation technique (BioDent) considers the relative indentation between the first and the last

cycle as a predictor of a single-value characterization of toughness in human bone ([Diez-Perez et al., 2010](#)), but in mouse bone this methodology for measuring single-value toughness needs further investigation ([Carriero et al., 2013](#), [Gallant et al., 2013](#)).

The methodology presented in this study seeks to provide a quantitative characterization of the resistance to crack propagation in mouse bone but naturally can be used also for testing other animal bones having a similar cylindrical cross-section as mouse femur. It is particularly advisable to use this method for small animal bones (e.g., mice, rats and guinea pigs), where milling beam samples out of their bone represents a limitation due to size constraints. In large

animal or human bone, testing conventional beam samples following ASTM standards (ASTM E1820-09, ASTM D790-10) allows more samples to be examined for fracture or other type of tests and provide a more accurate estimation of the fracture toughness due to their rectangular cross-section.

The R-curves based on stress-intensity measurements of the toughness used in this current study for mouse bone assume a cylindrical shape for the bone samples. This geometrical approximation might introduce some uncertainty in the toughness assessment. However, because the major and minor diameter of the bone do not differ by more than 35%, the error introduced by the geometrical approximation is generally small and the K-solution used still represents the most appropriate solution for calculating the toughness in this case. Another factor is that as mouse bones are physically small, there is always concern whether the assumptions of linear elasticity (i.e., a state of small-scale yielding) are met such that the K-based approach to characterizing crack initiation and propagation is appropriate. However, as can be seen in Fig. 3a, the K-based characterization was valid for all crack initiation data and for the crack growth results along the R-curve, except at crack extensions in excess of  $\sim 250\ \mu\text{m}$  in the WT bones. We additionally computed R-curves for mouse bone using the traditional work of fracture, which accounts for all modes of deformation and is not subject to the validity criteria imposed in fracture mechanics when defining the role of characterizing parameters such as K and J. We believe that the combination of both K-based and work of fracture  $W_f$  measurements of the R-curve offers the most feasible solution for evaluating the fracture properties of physically small mouse bones.

With the technique presented here, it is possible to visualize whether the toughening mechanisms observed in human bone, such as crack deflections, are also characteristic of mouse bone. Previous studies have shown that bone fracture is the result of intrinsic damage mechanisms, e.g., collagen fibrillar sliding and microcracking, ahead of the crack tip, that promote plasticity and therefore cracking, and extrinsic shielding mechanisms, e.g., crack deflection and bridging, that act to impede cracking (Launey et al., 2010). The origin of these two classes of toughening mechanisms arises at very different length-scales, with intrinsic toughening being primarily associated with processes, such as fibrillar sliding, at nanometer dimensions, in contrast to extrinsic toughening which is associated largely with the path of the crack and its interaction with features of the bone-matrix structures at the scale of 1 to several hundred micrometers. In this manner, changes in the bone toughness can be independently related to differing contributions in the intrinsic and extrinsic mechanisms. Because mice are often considered as models of human bone diseases, real-time visualization of the formation and propagation of cracks in their bones can reveal how diseases cause changes in the bone-matrix toughness and hence in the activity of corresponding toughening mechanisms with a resulting effect on fracture risk.

As noted, this technique additionally allows investigation into whether fracture toughness mechanisms in mouse bone differ from human bone; confirming that the fracture

toughness in mouse bone, which lacks the osteonal structure of human bone, has similar toughening mechanisms is important if mouse bone is to be used as a model for human bone fracture. From our results, it is clear that the absence of cement lines in mouse bone does not limit the degree of toughening. In human bones, these 'glue lines' (Von Ebner 1875) are the preferred sites for microcracks which generate weaknesses in the bone where the cracks would deflect or arrest (Yeni and Norman 2000). A similar crack deflection/twisting mechanism is present in the WT mouse bone in our study and lamellae interfaces may be providing this function. Previous studies showed that in human and mammalian bone the lamellae interfaces can generate toughness mechanisms, such as uncracked-ligament bridging (Nalla et al., 2003) and microcracks (Ziopoulos et al., 1996, 1999; Taylor et al., 2007) for crack propagating along the longitudinal direction of the bone, and crack deflection (Peterlik et al., 2006) and twisting (Koester et al., 2008), for cracks growing along the transverse direction. Accordingly, we believe that reduced and disorganized lamellar structure such as in *oim/+* bones (Saban et al., 1996; Carriero et al., 2014b), may explain the absence of deflections and twists of the crack paths in these bones.

Furthermore, WT bone is anisotropic and its crack deviation due to the lamellar structure suggests anisotropic damage criterion and elasticity, as showed by Feerick et al. (2013). In *oim/+* cortical bone instead, the presence of disorganized micro-lamellae that constantly change their orientation (Saban et al., 1996), is in agreement with the undeflected crack that suggests material isotropy and isotropic fracture criterion. Microstructure alignment and load influence the fracture toughness of bone (Zimmermann et al., 2009, 2010), and in turn can have further clinical implications for example in designing orthopedic screws and implant devices (Feerick and McGarry 2012), when the information is translated from mouse bone to human bone.

---

## 5. Conclusions

The *in situ* ESEM stable crack propagation technique presented in this study for mouse bones has been designed to provide important insight into how the bone fractures by showing the interaction between the stable crack and the bone-matrix structure during crack propagation. This *in situ* methodology allows identification of the onset of fracture in mouse bone (i.e., at the micro-notch surface or root), the micro-evolution of the damage (i.e., through the osteocyte lacunae or canals) and the toughening mechanisms (i.e., by forming deflecting cracks, microcracks or crack bridging). Furthermore, simultaneous high-resolution images of the crack path and real-time toughness measurements permit the identification of the salient sources of toughness and how these mechanisms actually confer crack-growth resistance to the bone. Indeed, this study presents the methodology for the analysis of fracture mechanics and crack resistance behavior (R-curve) of physiologically relevant stable crack propagation in mouse bone. The implementation of this methodology in understanding the mechanisms by which mouse bone toughness and interpreting these in terms of human bone

toughness can enhance the progress of pre-clinical testing for translational medicine aimed to reduce bone fracture risks.

## Acknowledgments

This work was performed primarily at the Lawrence Berkeley National Laboratory. It was funded by The Royal Academy of Engineering (Global Research Award for A.C.), by the Elsie Widdowson Foundation, UK (for S.J.S), and by the National Institute of Health (NIH/NIDCR) under Grant no. 5R01 DE015633 (for E.A.Z. and R.O.R.).

## REFERENCES

- Aspray, T.J., Prentice, A., Cole, T.J., Sawo, Y., Reeve, J., Francis, R.M., 1996. Low bone mineral content is common but osteoporotic fractures are rare in elderly rural Gambian women. *J. Bone Miner. Res.* 11, 1019–1025.
- ASTM D790-10, 2010. Standard test method for flexural properties of reinforced plastics and electrical insulation materials, Annual Book of American Society for Testing and Material Standards. ASTM International, West Conshohocken, PA.
- ASTM E1820-09, 2006. Standard test method for measurement of fracture toughness, Annual Book of American Society for Testing and Material Standards. ASTM International, West Conshohocken, PA.
- Barth, H.D., Launey, M.E., MacDowell, A.A., Ager 3rd, J.W., Ritchie, R.O., 2010. On the effect of X-ray irradiation on the deformation and fracture behavior of human cortical bone. *Bone* 46, 1475–1485.
- Busse, B., Bale, H.A., Zimmermann, E.A., Panganiban, B., Barth, H.D., Carriero, A., Vettorazzi, E., Zustin, J., Hahn, M., Ager 3rd, J.W., Puschel, K., Amling, M., Ritchie, R.O., 2013. Vitamin D deficiency induces early signs of aging in human bone, increasing the risk of fracture. *Sci. transl. Med.*, 193ra88.
- Carriero, A., Bruse, J.L., Shefelbine, S.J., 2013. Is microindentation indicative of fracture toughness in mouse bone? In: Proceedings of the 59th Annual Meeting of the Orthopaedic Research Society, San Antonio.
- Carriero, A., Doube, M., Vogt, M., Busse, B., Zustin, J., Levchuk, A., Schneider, P., Muller, R., Shefelbine, S.J., 2014a. Altered lacunar and vascular porosity in osteogenesis imperfecta mouse bone as revealed by synchrotron tomography contributes to bone fragility. *Bone* 61, 116–124.
- Carriero, A., Zimmermann, E.A., Paluszny, A., Tang, S.Y., Bale, H., Busse, B., Alliston, T., Kazakia, G., Ritchie, R.O., Shefelbine, S.J., 2014b. How tough is brittle bone? Investigating osteogenesis imperfecta in mouse bone. *J. Bone Miner. Res.* 29, 132–401.
- Christen, D., Levchuk, A., Schori, S., Schneider, P., Boyd, S.K., Muller, R., 2012. Deformable image registration and 3D strain mapping for the quantitative assessment of cortical bone microdamage. *J. Mech. Behav. Biomed. Mater.* 8, 184–193.
- Diez-Perez, A., Guerri, R., Noguez, X., Caceres, E., Pena, M.J., Mellibovsky, L., Randall, C., Bridges, D., Weaver, J.C., Proctor, A., Brimer, D., Koester, K.J., Ritchie, R.O., Hansma, P.K., 2010. Microindentation for in vivo measurement of bone tissue mechanical properties in humans. *J. Bone Miner. Res.* 25, 1877–1885.
- Feerick, E.M., McGarry, J.P., 2012. Cortical bone failure mechanisms during screw pullout. *J. Biomech.* 45, 1666–1672.
- Feerick, E.M., Liu, X.C., McGarry, P., 2013. Anisotropic mode-dependent damage of cortical bone using the extended finite element method (XFEM). *J. Mech. Behav. Biomed. Mater.* 20, 77–89.
- Gallant, M.A., Brown, D.M., Organ, J.M., Allen, M.R., Burr, D.B., 2013. Reference-point indentation correlates with bone toughness assessed using whole-bone traditional mechanical testing. *Bone* 53, 301–305.
- Heaney, R.P., 2003. Is the paradigm shifting? *Bone* 33, 457–465.
- Hui, S.L., Slemenda, C.W., Johnston Jr., C.C., 1988. Age and bone mass as predictors of fracture in a prospective study. *J. Clin. Invest.* 81, 1804–1809.
- Koester, K.J., Ager, J.W., Ritchie, R.O., 2008. The true toughness of human cortical bone measured with realistically short cracks. *Nat. Mater.* 7, 672–677.
- Kruzic, J.J., Kuskowski, S.J., Ritchie, R.O., 2005. Simple and accurate fracture toughness testing methods for pyrolytic carbon/graphite composites used in heart-valve prostheses. *J. Biomed. Mater. Res. A* 74, 461–464.
- Kruzic, J.J., Kim, D.K., Koester, K.J., Ritchie, R.O., 2009. Indentation techniques for evaluating the fracture toughness of biomaterials and hard tissues. *J. Mech. Behav. Biomed. Mater.* 2, 384–395.
- Launey, M.E., Buehler, M.J., Ritchie, R.O., 2010. On the mechanistic origins of toughness in bone. *Annu. Rev. Mater. Res.* 40, 25–53.
- Nalla, R.K., Kinney, J.H., Ritchie, R.O., 2003. Mechanistic fracture criteria for the failure of human cortical bone. *Nat. Mater.* 2, 164–168.
- Nalla, R.K., Kruzic, J.J., Ritchie, R.O., 2004a. On the origin of the toughness of mineralized tissue: microcracking or crack bridging? *Bone* 34, 790–798.
- Nalla, R.K., Kruzic, J.J., Kinney, J.H., Ritchie, R.O., 2004b. Effect of aging on the toughness of human cortical bone: evaluation by R-curves. *Bone* 35, 1240–1246.
- Nalla, R.K., Kruzic, J.J., Kinney, J.H., Ritchie, R.O., 2005. Mechanistic aspects of fracture and R-curve behavior in human cortical bone. *Biomaterials* 26, 217–231.
- Peterlik, H., Roschger, P., Klaushofer, K., Fratzl, P., 2006. From brittle to ductile fracture of bone. *Nat. Mater.* 5, 52–55.
- Riggs, B.L., Melton 3rd, L.J., O'Fallon, W.M., 1996. Drug therapy for vertebral fractures in osteoporosis: evidence that decreases in bone turnover and increases in bone mass both determine antifracture efficacy. *Bone* 18, 197S–201S.
- Ritchie, R.O., Koester, K.J., Ionova, S., Yao, W., Lane, N.E., Ager 3rd, J.W., 2008. Measurement of the toughness of bone: a tutorial with special reference to small animal studies. *Bone* 43, 798–812.
- Saban, J., Zussman, M.A., Havey, R., Patwardhan, A.G., Schneider, G.B., King, D., 1996. Heterozygous oim mice exhibit a mild form of osteogenesis imperfecta. *Bone* 19, 575–579.
- Taylor, D., Hazenberg, J.G., Lee, T.C., 2007. Living with cracks: damage and repair in human bone. *Nat. Mater.* 6, 263–268.
- Vashishth, D., Behiri, J.C., Bonfield, W., 1997. Crack growth resistance in cortical bone: concept of microcrack toughening. *J. Biomech.* 30, 763–769.
- Vashishth, D., Tanner, K.E., Bonfield, W., 2003. Experimental validation of a microcracking-based toughening mechanism for cortical bone. *J. Biomech.* 36, 121–124.
- Voide, R., Schneider, P., Stauber, M., Wyss, P., Stambanoni, M., Sennhauser, U., van Lenthe, G.H., Muller, R., 2009. Time-lapsed assessment of microcrack initiation and propagation in murine cortical bone at submicrometer resolution. *Bone* 45, 164–173.
- Von Ebner, V., 1875. Über den Feineren bau der Knochensubstanz, 72. Sitzungsberichte Deutsch Akad Wissenschaften, Berlin49.
- Yeni, Y.N., Brown, C.U., Wang, Z., Norman, T.L., 1997. The influence of bone morphology on fracture toughness of the human femur and tibia. *Bone* 21, 453–459.
- Yeni, Y.N., Norman, T.L., 2000. Calculation of porosity and osteonal cement line effects on the effective fracture toughness of cortical bone in longitudinal crack growth. *J. Biomed. Mater. Res.* 51, 504–509.

- Zahoor, A., 1989. In: *Ductile Fracture Handbook*. Electric Power Research Institute, Palo Alto 2–16.
- Zimmermann, E.A., Launey, M.E., Barth, H.D., Ritchie, R.O., 2009. Mixed-mode fracture of human cortical bone. *Biomaterials* 30, 5877–5884.
- Zimmermann, E.A., Launey, M.E., Ritchie, R.O., 2010. The significance of crack-resistance curves to the mixed-mode fracture toughness of human cortical bone. *Biomaterials* 31, 5297–5305.
- Zioupos, P., Currey, J.D., 1994. The extent of microcracking and the morphology of microcracks in damaged bone. *J. Mater. Sci.* 29, 978–986.
- Zioupos, P., Wang, X.T., Currey, J.D., 1996. The accumulation of fatigue microdamage in human cortical bone of two different ages in vitro. *Clin. Biomech. (Bristol, Avon)* 11, 365–375.
- Zioupos, P., 1999. On microcracks, microcracking, in-vivo, in vitro, in-situ and other issues. *J. Biomech.* 32 (209-11), 13–59.